Nuclear Instruments and Methods in Physics Research 218 (1983) 347–353
North-Holland, Amsterdam



# LIQUID METAL ION SOURCES: MECHANISM AND APPLICATIONS

L.W. SWANSON

*Oregon Graduate Center, Department of Applied Physics and Electrical Engineering, 19600 N.W. Walker Road, Beaverton, Oregon 97006, USA*

The emission characteristics, e.g. energy spread, energy deficit, and $M^{2+}/M^{+}$ ratios from Al, Ga, In, Bi and $Au_{90}Si_{10}$ liquid metal ion sources (LMIS) are discussed in terms of a field evaporation/postionization mechanism. It is shown that this model of LMIS is generally supported by the results. Focused beam results are presented which suggest a Gaussian source size for a Ga LMIS < 500 Å. It is shown that the best focused beam performance, i.e. maximum target current density for a specific beam size, is generally achieved at the lowest possible value of total current.

## 1. Introduction

Interest in the liquid metal ion source (LMIS) has been increasing rapidly due to its potential applications in microcircuit fabrication and various analytical microprobe instruments. Typically, an axial current intensity in excess of 20 $\mu$A/sr can be realized from a LMIS in the 1–10 $\mu$A range of total current. If the virtual source size, which is still a matter of discussion, is < 500 Å then a source brightness of $> 1 \times 10^6$ A/cm$^2 \cdot$ sr can be expected.

For microprobe applications, one is interested not only in source brightness, but also in the energy spread and its dependence on various source parameters. It is now well established that the minimum beam energy spread for the LMIS is $\gtrsim 5$ eV and strongly dependent on total current and charge-to-mass ratio of the ion [1,2]. Thus, chromatic aberrations limit the achievable beam size in most microprobe applications.

A further limit to achieving focused beam sizes < 0.1 $\mu$m is the virtual source size $d_g$ for the LMIS. This has not been established, however focused ion beam results to be presented here and elsewhere [3] suggest $d_g \lesssim 500$ Å.

In this paper we will review the current understanding of the ion formation mechanism in the LMIS and its relationship to beam energy spread and angular intensity.

## 2. Ion formation mechanism

The LMIS consists of a low volatility liquid metal film flowing to the apex of a solid needle support structure whose apex radius is ~ 1–5 $\mu$m [4]. The application of an electric field of sufficient strength will deform the liquid film on the needle apex into a conical protrusion as shown in fig. 1 for a Bi LMIS that was solidified during operation and photographed in an SEM. As shown by Taylor [5], the cone can be stabilized by the static balance between the surface tension and electrostatic forces when the cone half-angle is 49.3°.

The liquid cone apex radius is undetermined by the Taylor theory and, as shown in fig. 1, attains a value < 500 Å. It can be shown that the cone apex is unstable with respect to further elongation until hydrodynamic and space charge considerations stabilize the cone apex at a particular radius [6,7]. The exact value of the apex radius and the detailed shape of the cone in the apex region is a matter still being resolved [7]. As will be shown, a field evaporation mechanism for ion formation requires typically an apex field strength $F_a$ of ~ 2 V/Å. In order to achieve this field strength with a Taylor cone geometry it can be shown that the apex radius $r_a$ must be ~ 20 Å [6,7]. Kang and Swanson [7], using a computer based, numerical solution of the Poisson equation for the Taylor cone geometry, showed that a field of 2 V/Å cannot be maintained at the emitter apex for total currents $I_T \gtrsim 2$ $\mu$A and $r_a < 50$ Å due to space charge suppression. Only by assuming an elongation near the apex of the Taylor cone can values of $I_T > 2$ $\mu$A be realized with $F_a = 2$ V/Å. Thus, it appears that during operation some deviation from the fig. 1 shape occurs. This has been verified recently by transmission electron microscope examination of the apex of the LMIS source during operation [8].

The field evaporation mechanism of ion formation is shown schematically in fig. 2. For the so-called "image hump" model, i.e. evaporation of the ion over the Schottky barrier formed by the field acting on the $M^+$ state ion, it can be shown that the activation barrier $Q(F)$ for formation of a singly charged ion is given by

$$Q(F) = H_0 + I_1 - \phi - 3.8F^{1/2}, \qquad (1)$$

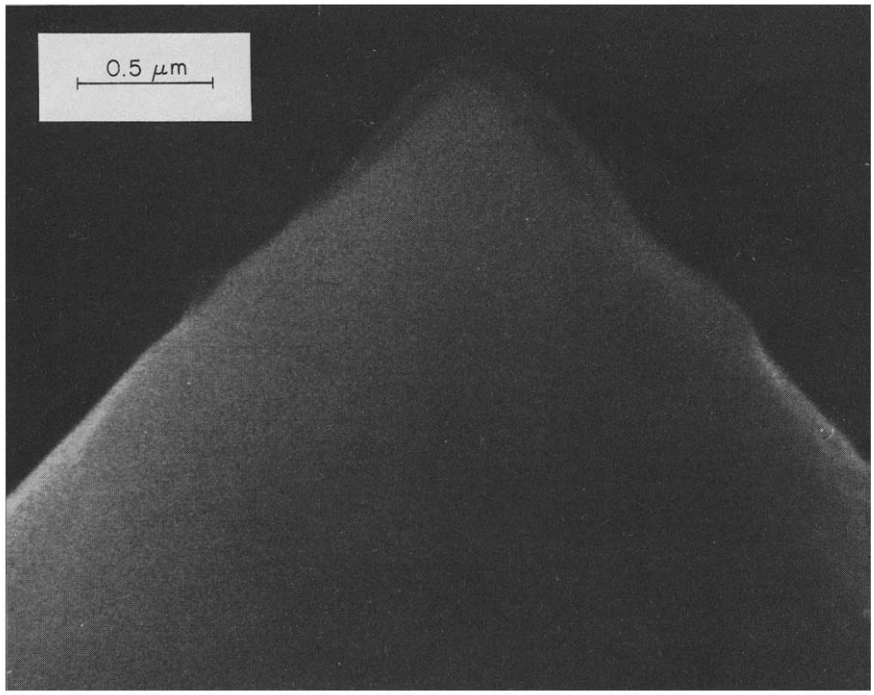


Fig. 1. SEM photo of a "frozen" Bi Taylor cone.

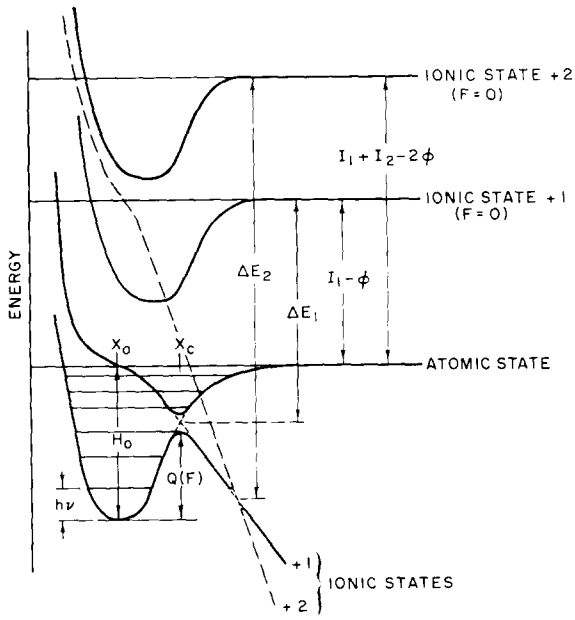


Fig. 2. Potential energy diagram showing field evaporation of $M^+$ and $M^{2+}$ ions. The respective energy deficits are $\Delta E_1$ and $\Delta E_2$.

where the binding energy of the metal $H_0$, its work function $\phi$ and the ionization potential $I_1$ are in eV and $F$ is in V/Å. Higher charged states are believed to be formed by positionization as shown schematically in fig. 2 for $M^+ \rightarrow M^{2+}$. Postionization (PI) transition probabilities for a variety of ions as a function of $F$ have been calculated by Kingham [9] and can be used as a determination of $F_{PI}$ if $M^n/M^{n+1}$ is determined experimentally. Also, if one assumes $Q(F) \equiv 0$, i.e., $T = 0$ K, the value of $F^+$ for singly charged ion formation can be calculated from eq. (1).

A further prediction of the field evaporation mechanism is the value of the energy deficit, $\Delta E_n$, i.e., the amount of energy gained or lost relative to the full potential drop between the emitter and extractor electrodes. The value of $\Delta E_n$ for an ion of charge $n$ is given by (see fig. 2)

$$\Delta E_n = H_0 + \sum_1^n I_n - n\phi_c - Q(F), \qquad (2)$$

where $\phi_c$ is the work function of the retarding electrode and $I_n$ is the ionization potential of the $n$th charged state.

## 3. Mass spectrometer studies of various LMIS

From mass spectrometer studies of LMIS using the experimental arrangement shown in fig. 3 it is possible

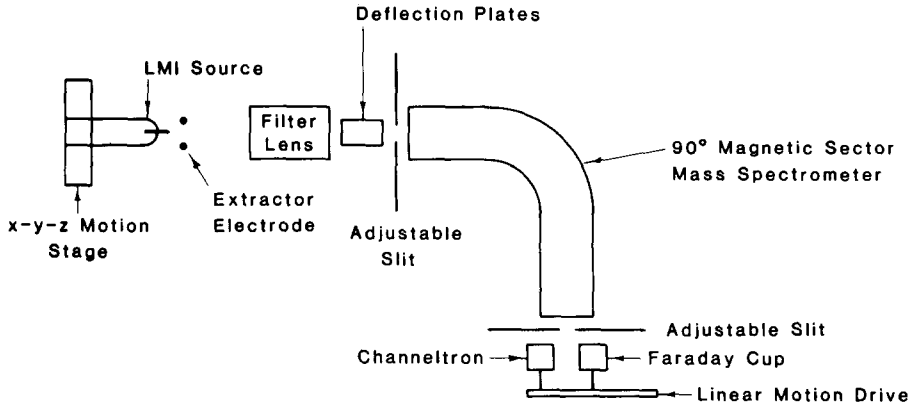


Fig. 3. Experimental arrangement of the mass spectrometer and saddle point filter lens for energy distribution measurement.

to determine not only the relative amount of the various charge to mass species, but also the energy distribution and energy deficits as a function of emitter temperature and total current $I_T$. Such studies have been carried out in part for the LMIS indicated in table 1.

### 3.1. Measured $M^{2+}/M^{+}$ ratios

For most of the pure metal LMIS in table 1 excluding Au, the values of $F^+$ and $F_{PI}$ are in reasonable agreement and are all close to 2.0 V/Å. The reason pure Au gives $F_{PI} < F^+$ may be due to the fact that some $Au^+$ arises from both field evaporation and gas phase field ionization several tens of Å from the apex due to the high v.p. of Au at its melting temperature. The $M^+$ arising from field ionization would not be subject to postionization since the field is too low where $Au^+$ is formed. A similar result seems to be occurring for $Si^+$ in the $Au_{90}Si_{10}$ LMIS and thereby reducing the observed $M^{2+}/M^+$ and $F_{PI}$ values from what would be expected for pure field evaporation. Fig. 4 shows the appearance of a low energy shoulder on the $Si^+$ total energy distribution (TED) presumably due to ion formation several Å out from the emitter surface. A similar result has been observed for $Ga^+$ at $T > 500$ K [1], $Au_2^+$, $Au_3^{2+}$ [10] and for $AuSi^+$ species in the $Au_{90}Si_{10}$ LMIS. It is somewhat surprising that field ionization can occur at the apparent low temperature of an $Au_{90}Si_{10}$ LMIS since the vapor pressure would be much too low to produce a sufficiently high vapor density of neutrals. Presumably, other mechanisms for neutral species production must be operative. Thus, the disagreement in

Table 1
Properties and $M^{2+}/M^+$ ratios at 10 μA for the indicated LMIS. Calculated fields $F^+$ for ion formation [calculated from eq. (1) for $Q(F) = 0$] and $F_{PI}$ for post-ionization to give $M^{2+}/M^+$ ratios are indicated.

| | $T_{m.p.}$ (K) | $F^+$ (V/Å) | $M^{2+}/M^+$ ($I = 10$ μA) [c] | $F_{PI}$ (V/Å) |
|---|---|---|---|---|
| Al | 933 ($4.9\times10^{-9}$) [a] | 1.8 | $2.2\times10^{-3}$ | 2.0 |
| Ga | 302 ($6.8\times10^{-41}$) | 1.6 | $9\times10^{-5}$ | 2.1 |
| In | 429 ($1.9\times10^{-21}$) | 1.4 | $2\times10^{-5}$ | 1.7 |
| Au | 1336 ($6.4\times10^{-6}$) | 5.1 | 1.5 | 3.5 |
| Bi | 544 ($6\times10^{-11}$) | 2.3 | $2.3\times10^{-2}$ | 1.9 |
| Si (in $Au_{90}Si_{10}$) | 930 | 4.2 [b] | 2.9 | 2.0 |
| Au (in $Au_{90}Si_{10}$) | 930 | 5.1 [b] | 4.6 | 3.7 |

[a] V.P. in Torr at melting temperature.
[b] Based on pure metal values.
[c] Measurements based on mass spectrometer peak areas.

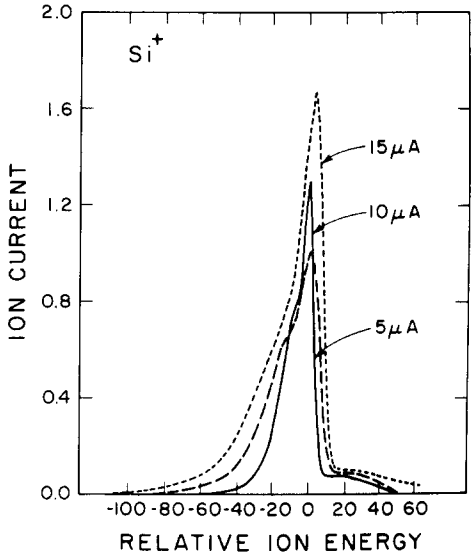


Fig. 4. Energy distribution curve for $Si^+$ at the indicated total currents.

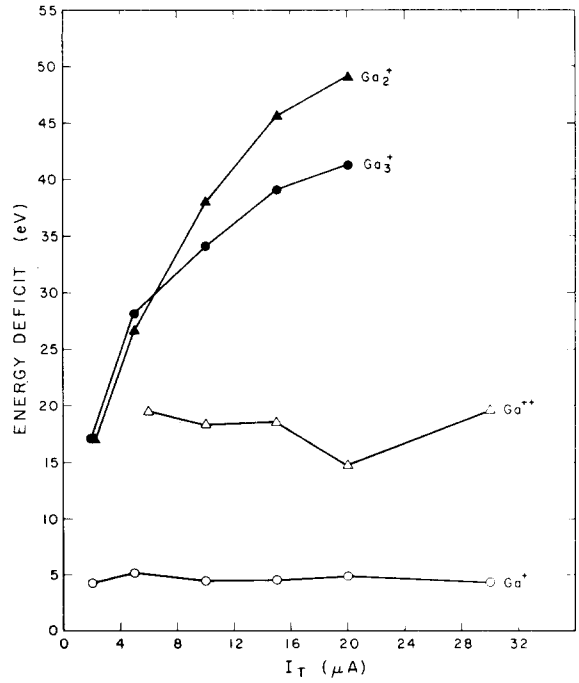


Fig. 5. Energy deficit measurements vs total current for the indicated Ga species.

$F_{PI}$ values for Au and Si in $Au_{90}Si_{10}$ in table 1 is believed due to a contribution to the $M^+$ rate of formation from a mechanism other than field evaporation.

### 3.2. Energy deficit measurements

Another verification of the field evaporation mechanism at low values of total current $I_T$ is the value of the energy deficit $\Delta E_n$ for the monomer ions of the pure metal sources. Table 2 compares the experimental value of $\Delta E_n$ (obtained by extrapolation to $I_T = 0$) with those predicted by eq. (2) where it was assumed that $Q(F) = 0$. Again the agreement between the calculated and measured values of $\Delta E_n$ is supportive of a field evaporation mechanism of ion formation.

Typically for the pure metal sources Al, Ga, In and Bi the energy deficits for the much smaller yields of cluster ions $M_n^+$ are large when compared with the $M^+$ and $M^{2+}$ ions and increase rapidly with $I_T$ as shown in fig. 5 for Ga. As pointed out earlier by Culbertson et al. [11], these results along with the larger energy spreads associated with the $M_n^+$ species are suggestive of a field ionization mechanism of ion formation for these species.

Table 2
Comparison of energy deficits $\Delta E_n$ calculated by eq. (2) [assuming $C(F) = 0$] and measured by extrapolating experimental results to $I_T = 0$.

| Ion | $\Delta E_n$ (Calc.) (eV) | $\Delta E_n$ (Exp.) (eV) |
|---|---|---|
| $Al^+$ | 5.0 | $3.6 \pm 1$ |
| $Ga^+$ | 4.9 | $3.4 \pm 1$ |
| $Ga^{++}$ | 21.5 | $19 \pm 1$ |
| $In^+$ | 5.8 | $3.2 \pm 1$ |
| $Bi^+$ | 6.0 | $4.7 \pm 1$ |

### 3.3. Energy spread results

The total energy distribution of various species in the LMIS can be compared by measuring the full width of the energy distributions at half maxima ($\Delta E_{fwhm}$) as a function of total current. Figs. 6 and 7 give such results for the table I LMIS. It is apparent that $\Delta E_{fwhm}$ increases with $I_T$ and mass charge ratio $m/q$. Extrapolation of the $\Delta E_{fwhm}$ curves to $I_T = 0$ suggests $\Delta E^0_{fwhm} \cong 5$ and 3 eV for $M^+$ and $M^{2+}$ species respectively. Again, these results are consistent with a field evaporation mechanism where the $M^+$ and $M^{2+}$ ions, according to fig. 2, are formed in a narrow range of distance $\Delta x$ from the surface of electric neutrality. Roughly speaking $\Delta x \sim \Delta E^0_{fwhm}/F$ which means $\Delta x \cong 1.5$–$2.5$ Å for the $M^{2+}$ and $M^+$ ions respectively. This range of values of $\Delta x$ is larger than what might be expected for a field evaporation mechanism and may be due to the general current dependent broadening mechanism obvious in the figs. 6 and 7 results.

The unusual result for $Si^+$ in fig. 2 stems from the low energy shoulder on the TED as seen in fig. 4. Presumbly, if the low energy peak were subtracted, the

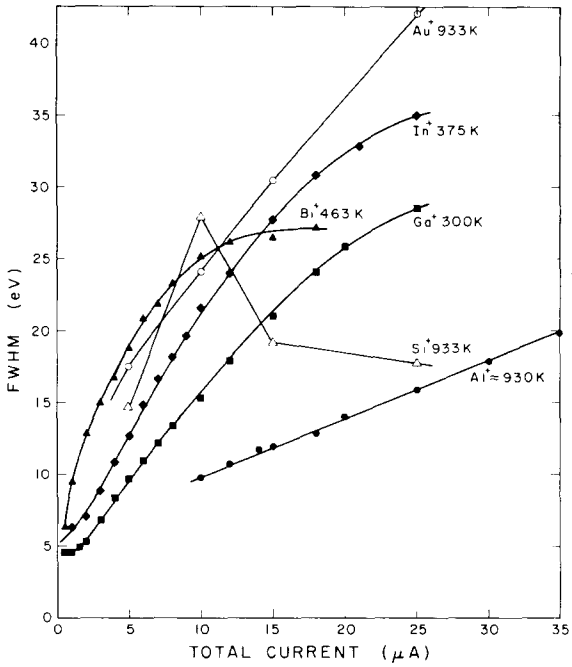


Fig. 6. Full width at half-maximum (fwhm) values vs total current measured from the energy distribution curves of the indicated species. The Au and Si results were obtained from an $Au_{90}Si_{10}$ alloy.

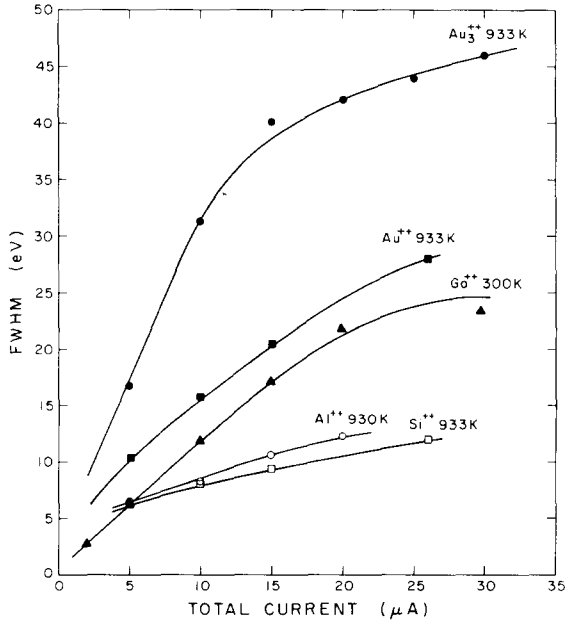


Fig. 7. Full width at half-maximum (fwhm) values vs total current measured from the energy distribution curves of the indicated species. The Au and Si results were obtained from an $Au_{90}Si_{10}$ alloy.

fig. 6 $Si^+$ TED results would show a monotonic increase of $\Delta E_{\mathrm{fwhm}}$ with $I_{\mathrm{T}}$.

For the field evaporated and postionized species we obtain empirically that

$$\Delta E^{\mathrm{c}}_{\mathrm{fwhm}} = k(m/q)^{1/2} I_{\mathrm{T}}^{0.6}, \tag{3}$$

where $\Delta E^{\mathrm{c}}_{\mathrm{fwhm}} = [\Delta E^{2}_{\mathrm{fwhm}} - \Delta E^{02}_{\mathrm{fwhm}}]^{1/2}$. The eq. (3) relationship is believed to arise from the random density fluctuations in the beam which can be shown to cause an increase in $\Delta E_{\mathrm{fwhm}}$ through Coulomb interactions among the emitted particles [12].

## 4. Focused beam results

The important source parameters so far as focused beam results are concerned are the beam energy spread $\Delta E_{\mathrm{fwhm}}$, the angular beam intensity $\mathrm{d}I/\mathrm{d}\Omega$ and the Gaussian source size $d_{\mathrm{g}}$ of the beam. Typically only $d_{\mathrm{g}}$ and chromatic aberration contribute significantly to the focused beam size $d$. Thus we can write in the customary fashion

$$d^2 = M^2\left(d_{\mathrm{g}}^2 + d_{\mathrm{c}}^2\right), \tag{4}$$

where

$$d_{\mathrm{c}} = C_{\mathrm{c}}\alpha_0 \Delta V / V_0, \tag{5}$$

and $C_{\mathrm{c}}$ is the chromatic aberration referred to the object side of the lens and $\alpha_0$ and $V_0$ are the object side aperture half-angle and emitter extraction voltage respectively. The beam energy spread $\Delta V$ is not symmetrical for all species. Since the beam current $I_{\mathrm{p}}$ is related to

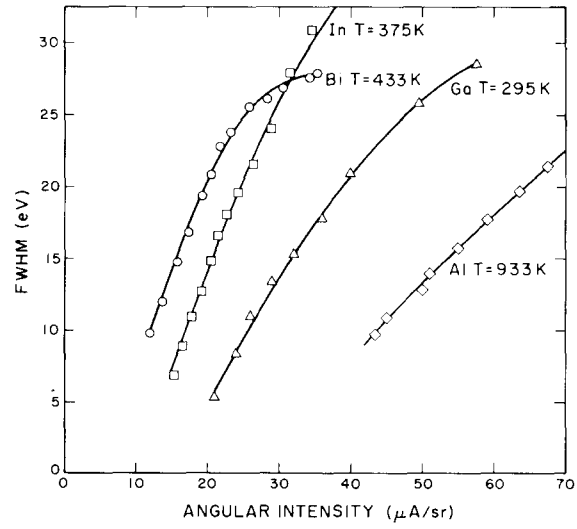


Fig. 8. Full width at half-maximum (fwhm) values of the energy distribution vs angular intensity for the indicated LMIS.

the angular intensity $dI/d\Omega$ as

$$I_p = \frac{dI}{d\Omega}\pi\alpha_0^2, \tag{6}$$

one can obtain from eqs. (4)–(6)

$$I_p = \left(\frac{d^2}{M^2} - d_g^2\right)\left(\frac{V_0\pi}{\Delta V C_c}\right)^2 \frac{dI}{d\Omega}\pi. \tag{7}$$

Fig. 8 provides the experimental relationship between $dI/d\Omega$ and $\Delta V$ for several pure LMIS where the $M^+$ species is dominant. To optimize focused beam performance according to eq. (6) one must maximize $dI/(d\Omega\Delta V^2)$. It is clear from fig. 8 that the latter requirement is a sensitive function of mass; thus the value of $dI/d\Omega\Delta V^2$ for Al and Bi are 0.44 and 0.12 $\mu A/sr \cdot V^2$ respectively at the low values of $\Delta V^2$. Also, there is no gain in $I_p$ at a fixed $d$ by increasing $dI/d\Omega$ (i.e. increasing $I_T$), since $dI/(d\Omega\Delta V^2)$ decreases with increasing $dI/d\Omega$. Thus we are left with the curious conclusion that in order to increase $I_p$ at a fixed $d$ (i.e., increase $J_p$), one must operate at the lowest possible value of $I_T$. Also increasing $V_0$, while maintaining a low value of $C_c$ also improves performance according to eq. (7). The latter improvement is ultimately limited by voltage breakdown within the electrostatic lens.

Fig. 9 provides focused beam column performance for a three element voltage and physically asymmetric electrostatic lens column using a Ga LMIS. This lens, which is described elsewhere [13,14], has a low $C_c$ and when combined with an octupole electrostatic stigmator/deflector [15] constitutes a simple but effective focusing system. The value of $\alpha_0$ and $V_0$ were 2 mr and 14 kV respectively, $dI/d\Omega = 20$ $\mu A/sr$ and $\Delta V$ was assumed to be 5 eV.

Values of beam size in fig. 9 were obtained both by scanning across a gold coated knife edge made by directional etching of Si and by milling lines in a 0.1 $\mu$m thick Au coating on Si. Both methods gave good agreement for measurements of d vs beam voltage. As can be seen in fig. 9 results current densities of ~ 1 A/cm$^2$ in a 0.2 $\mu$m beam size can readily be achieved at 25 kV beam voltage and a large working distance.

Most interesting in fig. 9 is the comparison between experimental and calculated values of $d$ using various values of $d_g$. From the latter comparison one can conclude that $d_g < 500$ Å under the conditions of these measurements.

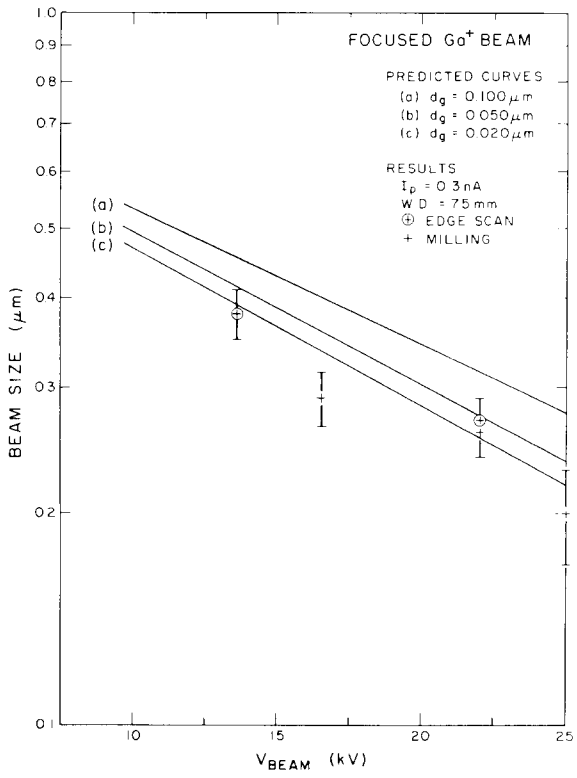


Fig. 9. Comparison of experimental and calculated focused beam size vs beam voltage. The indicated values of $d_g$ were used in the calculated curves.

## 5. Conclusions

Experimental measurements of the $M^{2+}/M^+$ ratios have been used with postionization theory [9] to give predicted values of the field strength for operating LMIS. Generally the predicted fields are in accordance with the values expected for a field evaporation mechanism for ion formation. For some LMIS, e.g. Au and $Au_{90}Si_{10}$, the results suggest an additional field ionization mechanism for $M^+$ formation. Energy deficit measurements also confirm a field evaporation and field ionization mechanism for $M^+$ and $M_n^+$ ions respectively for pure metal LMIS.

Focused ion beam results using a LMIS show that the largest value of current density is usually achieved at the lowest value of total source current. This is due to the increase in energy spread with both $m/q$ and $I_T$. Nonetheless a simple lens focusing column can provide ~ 1 A/cm$^2$ of $Ga^+$ in a 0.2 $\mu$m beam size at 25 kV beam energy.

This work was supported by a grant from the National Science Foundation (ECS-8206796) and by a grant from the Murdock Charitable Trust Foundation.

## References

[1] L.W. Swanson, G.A. Schwind and A.E. Bell, J. Appl. Phys. 51 (1980) 3453.

[2] A.E. Bell, G.A. Schwind and L.W. Swanson, J. Appl. Phys. 53 (1982) 4602.
[3] R.L. Seliger, J.W. Ward, V. Wang and R.L. Kubena, Appl. Phys. Lett. 34 (1979) 310.
[4] L.W. Swanson and G.A. Schwind, J. Appl. Phys. 49 (1978) 5655.
[5] G.I. Taylor, Proc. Roy. Soc. (London) A280 (1964) 383.
[6] R. Gomer, Appl. Phys. 19 (1979) 365.
[7] N.K. Kang and L.W. Swanson, Appl. Phys. A 30 (1983) 95.
[8] H. Gaubi, P. Sudraud, N. Tence and J. Van de Walle, Proc. 29th Int. Field emission Symp., Chalmers Univ., Göteborg, Sweden, (Almqvist and Wiksell, Stockholm, 1982) p. 357.
[9] D. Kingham, Surf. Sci. 116 (1982) 273.
[10] P. Sudraud, C. Colliex and J. Van de Walle, J. de Phys. Lett. 40 (1979) L207.
[11] R.J. Culbertson, G.H. Robertson and T. Sakurai, J. Vac. Sci. Technol. 16 (1979) 1868.
[12] W. Kanuer, Optik 59 (1981) 335.
[13] J. Orloff and L.W. Swanson, J. Appl. Phys. 50 (1979) 2494.
[14] J. Orloff and L.W. Swanson, J. Vac. Sci. Technol. 19 (1981) 1149.
[15] J. Kelly, Adv. Electron. Phys. 43 (1979) 43.